Bandwidth efficient coherent lidar based on phase-diversity detection

Tongqing Liao,[1,2] Mahmood Hameed,[1] and Rongqing Hui[1,*]

[1]Department of Electrical Engineering and Computer Science, University of Kansas, Lawrence, Kansas 66045, USA

[2]School of Electronic and Information Engineering, Anhui University, Hefei 230009, Anhui Province, China

*Corresponding author: hui@ittc.ku.edu

Received 4 February 2015; revised 4 March 2015; accepted 6 March 2015;
posted 9 March 2015 (Doc. ID 232641); published 6 April 2015

Bandwidth efficient coherent lidar based on phase-diversity detection is reported for the first time, to the best of our knowledge, which allows the doubling of bandwidth efficiency through the simultaneous utilization of the in-phase (I) and quadrature (Q) components. By maintaining RF phase continuity between linearly frequency-chirped I and Q components through digital signal processing, the range resolution of the lidar system can be improved. © 2015 Optical Society of America

OCIS codes: (280.3640) Lidar; (060.2300) Fiber measurements; (120.4640) Optical instruments.
http://dx.doi.org/10.1364/AO.54.003157

1. Introduction

Light detection and ranging, known as lidar, is a popular remote sensing technique which can be used to measure a variety of parameters including distance, velocity, and vibration, as well as allowing for high-resolution mapping [1–4]. In comparison to radio-frequency (RF) remote sensing, lidar is able to provide much finer range resolution and spatial resolution because of its higher carrier frequency and smaller spot size at the foci. Various different modulation and detection techniques can be used for a lidar altimeter, and the range resolution is generally determined by $\Delta R = c/2B$, where c is the speed of light, and B is the modulation bandwidth [2]. A frequency-modulated continuous-wave (FMCW) lidar uses linearly frequency-chirped optical pulses with relatively long pulse duration, and thus the peak power of each optical pulse is much lower than that in a short-pulsed lidar with comparable range resolution [5–7]. Detection sensitivity, another important parameter of a lidar system, depends on the receiver configuration. Coherent detection has been shown to provide quantum-limited detection sensitivity, and in addition, it also allows the utilization of both the intensity and the phase of the optical signal, which provides an additional degree of freedom in lidar design and performance optimization.

Traditionally, the useful bandwidth of the FMCW optical signal is equal to the chirping bandwidth of the RF signal applied on the electro-optic modulator in the lidar transmitter, and thus wideband RF and high-speed digital components are required to achieve a fine range resolution. Reference [8] explored the possibility of utilizing sparse frequency linear frequency modulation (SF-LFM) for lidar applications. Reference [9] verified experimentally that SF-LFM lidar signals have the ability to increase the range resolution of a lidar system without the need of increasing the modulator bandwidth. In such an approach, multiple laser sources have to be used with feedback-locked optical frequencies. Another category of approaches is based on ultrawideband direct optical chirp generation through diode lasers [10,11], and ring resonators [12]. This technique is most suitable for applications that require submillimeter range resolution, which is similar to optical coherence tomography (OCT) [12].

In this paper, we demonstrate wideband direct RF chirping for lidar applications which has better

1559-128X/15/113157-05$15.00/0

controllability and flexibility than optical chirping techniques. We show that the chirp bandwidth of the optical signal can be twice as wide as that of the RF chirp when an in-phase/quadrature (I/Q) modulator is employed for electro-optic modulation, and the I and Q components can be separately detected with coherent homodyne detection based on a 90-degree optical hybrid [5,6]. More specifically, we demonstrate that 7 GHz continuous optical chirping, corresponding to a range resolution of approximately 1.28 cm, can be achieved with 3.5 GHz RF bandwidth. One important requirement permitting simultaneously utilizing both the I and the Q components of the optical signal is the phase continuity between the chirp waveforms carried by the upper and the lower sidebands, which can be maintained through signal processing. I/Q modulation, as well as the required signal processing, increase the overall complexity of the lidar system. A trade-off has to be made between system complexity and the performance improvement in practical applications.

2. Operation Principle and Experimental Setup

Figure 1 shows the experimental setup to prove the concept of the proposed lidar system. A fiber-pigtailed tunable laser assembly with 100 kHz spectral linewidth (Emcore TTX1994) was used as the light source which operated in continuous wave (CW) with the wavelength set at 1549.65 nm. The laser output was split into two parts by a fiber directional coupler, one part was sent into an I/Q electro-optic modulator, while the other part was sent directly to the receiver as the local oscillator (LO) for coherent homodyne detection.

An arbitrary waveform generator (AWG: Tektronix 70000A) with a 20 GS/s sampling rate was used to generate two linearly chirped RF waveforms as the in-phase and the quadrature signals to drive the I/Q modulator. The modulated optical signal is amplified by an erbium-doped fiber amplifier (EDFA). The amplified optical signal was delivered to a telescope through another fiber coupler which helped redirect the reflected optical signal from the target back to the coherent receiver. The target is made of a retro-reflective tape which could move along a sliding rail, so that the distance between the telescope and target could be varied. The other output of the directional coupler was connected to a reflective fiber terminal through a fiber delay line and an optical attenuator. This allowed a controllable small portion

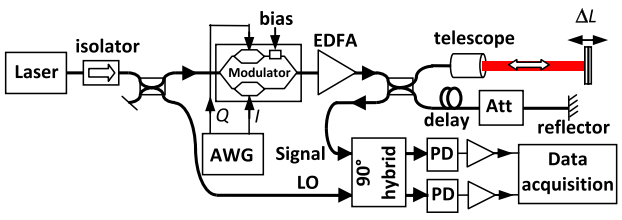

Fig. 1. Experimental setup. AWG, arbitrary waveform generator; Att, optical attenuator; PD, photodiode.

of the optical signal to be reflected back to the receiver as a reference for a fixed distance. In a practical lidar system, this second fiber directional coupler can be replaced by an optical circulator to avoid the splitting loss of the optical signal. A 90-degree optical hybrid was used in the coherent optical receiver to mix the optical signal and the LO into two separate photodiodes. Analog-to-digital conversion (ADC) and data acquisition were accomplished with a real-time oscilloscope (LeCory 8600A) with a 20 Gs/s sampling rate and 4 GHz analog bandwidth. Digital signal processing including complex spectrum reconstruction, digital equalization, and frequency down-conversion were conducted off-line through a MATLAB program.

A unique advantage of an I/Q modulator is the capability of introducing complex optical field modulation, which provides an additional degree of freedom compared to an intensity modulator. For a modulated optical pulse train with the pulse width T and pulse repetition time $T + \Delta T$, as illustrated in Fig. 2(a) (only shows two periods), the complex field modulation allows two independent linear chirp components to be loaded, one on each side of the optical carrier.

To create one wideband chirp waveform which linearly sweeps from f_1 to f_2 on the upper optical sideband, and the other wideband chirp waveform which linearly sweeps from f_2 to f_1 on the lower optical sideband, the two voltage waveforms used to drive I and Q arms of the I/Q modulator are [5]

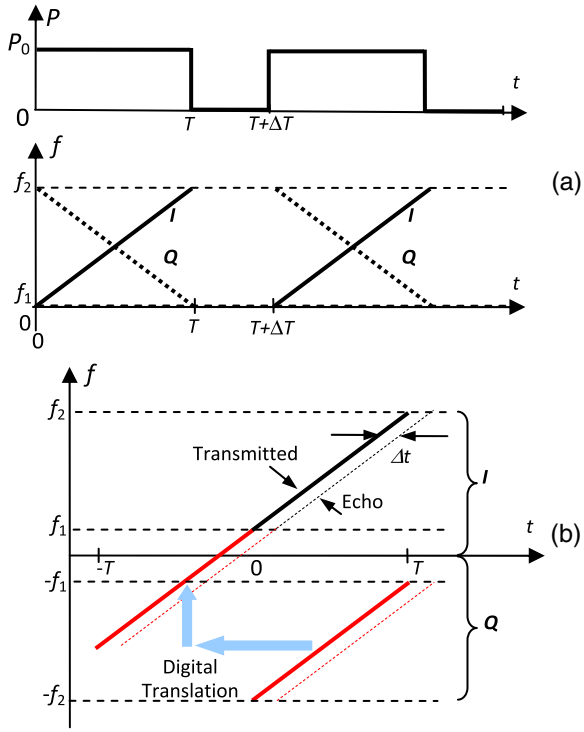

Fig. 2. Illustration of the linearly FM-chirp chirped signal for a bandwidth efficient coherent lidar. Transmitted chirps are represented by solid lines and the echo signal is represented by dashed lines. $T + \Delta T$ is the period and T is the pulse width.

$$V_I = V_D \cos\left(2\pi f_1 t + \pi \frac{f_2 - f_1}{T} t^2\right) - V_D \sin\left(2\pi f_2 t + \pi \frac{f_1 - f_2}{T} t^2\right), \quad (1)$$

$$V_Q = -V_D \sin\left(2\pi f_1 t + \pi \frac{f_2 - f_1}{T} t^2\right) + V_D \cos\left(2\pi f_2 t + \pi \frac{f_1 - f_2}{T} t^2\right), \quad (2)$$

where V_D is the amplitude of the driving voltage signal. An I/Q electro-optic modulator consists of two intensity modulators in the two arms of a Mach–Zehnder interferometer (MZI) configuration and a phase shifter between them. When both of the two intensity modulators inside the I/Q modulator are biased at the minimum transmission point, and the phase shifter is biased at the quadrature point of the MZI, the optical field at the output of the I/Q modulator is [5]

$$E_o = E_s \sin\left(\frac{\pi V_I}{V_\pi}\right) \cos(2\pi f_0 t) + E_s \sin\left(\frac{\pi V_Q}{V_\pi}\right) \sin(2\pi f_0 t), \quad (3)$$

where f_0 is the optical carrier frequency and E_s is the optical field amplitude at the modulator input, and V_π is the voltage required for the transfer function to change from the minimum to the maximum of each intensity modulator.

The optical field reflected from the target E_o contains a time delay Δt compared to the launched optical field, and the optical LO can be expressed as $E_{LO} = A_{LO} \cos(2\pi f_0 t)$, where A_{LO} is the field amplitude. Sending E_o and E_{LO} into the two input ports of the 90-degree hybrid and assuming the matched polarization states between the input optical signal and the LO, the photocurrents of the two photodetectors in the phase diversity receiver are

$$I_I(t) = \Re|E_I|^2 \propto \cos\left[2\pi\left(f_1 + \frac{f_2 - f_1}{2T}(t - \Delta t)\right)t - \frac{\pi}{4}\right] - \sin\left[2\pi\left(f_2 + \frac{f_1 - f_2}{2T}(t - \Delta t)\right)t + \frac{\pi}{4}\right], \quad (4)$$

$$I_Q(t) = \Re|E_Q|^2 \propto -\sin\left[2\pi\left(f_1 + \frac{f_2 - f_1}{2T}(t - \Delta t)\right)t - \frac{\pi}{4}\right] + \cos\left[2\pi t\left(f_2 + \frac{f_1 - f_2}{2T}(t - \Delta t)\right)t + \frac{\pi}{4}\right], \quad (5)$$

where $\Re$ is the responsivity of the photodiode, and terms due to direct detection have been neglected for simplicity. These two photocurrent signals can be digitized through ADCs and recorded. Since they represent the real and the imaginary parts of the optical signal, the complex optical field can be represented by

$$I_{\text{complex}}(t) = I_I(t) - jI_Q(t) \propto \exp\left[2\pi\left(f_1 + \frac{f_2 - f_1}{2T}(t - \Delta t)\right)t - \frac{\pi}{4}\right] - j\exp\left[2\pi\left(-f_2 - \frac{f_1 - f_2}{2T}(t - \Delta t)\right)t - \frac{\pi}{4}\right]. \quad (6)$$

Equation (6) can be reconstructed in the digital domain through signal processing. This complex waveform can be converted into frequency domain through a fast Fourier transform (FFT). Clearly, the two independently chirped RF waveforms are carried by the upper and the lower sidebands, respectively, as represented by the 1st and the 2nd terms on the right-hand side of Eq. (6), which can be separated in the signal processing.

3. Results and Discussion

In the experiment, we have set $f_1 = 0.5$ GHz and $f_2 = 4$ GHz so that the chirping bandwidth carried by each optical sideband was 3.5 GHz, and the pulse duration was set as 1 μs. Figure 3(a) shows typical RF spectra of the photocurrents measured from the I and the Q channels. The complex optical signal can be reconstructed as a complex electrical signal $I_{\text{complex}} = I_I - jI_Q$ and its spectrum is shown in Fig. 3(b), where the upper and the lower sidebands carry independent waveforms which can be dechirped separately in the digital process. To obtain the target range information, the upper and the lower sidebands of the complex RF spectrum have to be separated and each mixing with the original RF chirping waveform in the postprocessing. As illustrated in Fig. 2(a), each sideband of the complex optical carrier carries a chirping bandwidth of $|f_2 - f_1|$ within a pulse width T. Proper combination of waveforms carried by the upper and the lower sidebands can double the overall chirping bandwidth to $2|f_2 - f_1|$ in a temporal duration of $2T$. This effectively improves the range resolution by 50% without requiring increased RF bandwidth and digital processing speed.

Note that in order to realize the improvement of range resolution, phase continuity of the combined waveform is critically important. Since frequency chirping of each sideband starts from f_1, which is 0.5 GHz in our experiment, there is a frequency gap of $2f_1$ which would cause a phase discontinuity between waveforms of the upper and the lower sidebands when they combine. Since the phase of the RF chirping waveform is well defined by the AWG, this phase discontinuity can be corrected in the frequency down-conversion process. More specifically, the waveforms (both transmitted and echo from the target) acquired from one sideband have to be translated by T in time and $2f_1$ in frequency with respected to the waveforms of the other sideband as illustrated in Fig. 2. Additionally, special attention

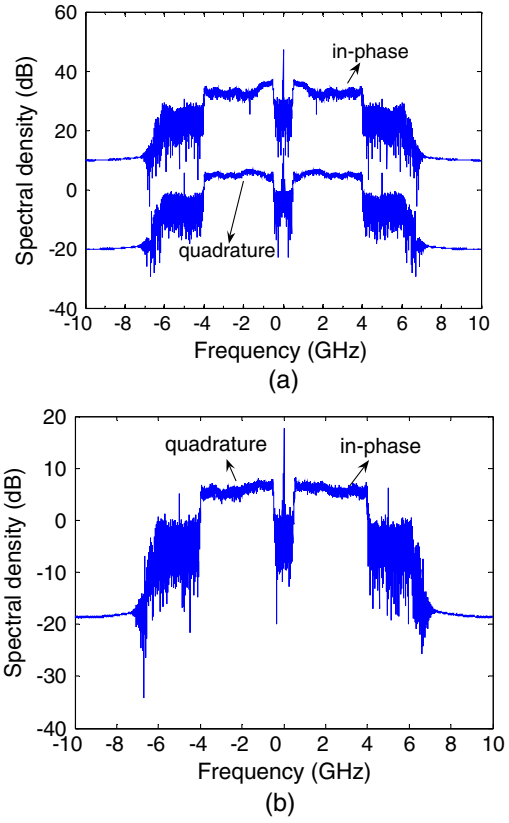

Fig. 3. Signal spectra measured with coherent heterodyne detection. (a) Spectra of the in-phase (top) and the quadrature channels (bottom), and (b) spectrum of the complex optical field.

has to be paid when synthesizing the waveform in the AWG to ensure an equal phase at the beginning and the end of the waveform.

To illustrate the impact of phase discontinuity Fig. 4 shows the down-converted RF spectra of waveforms composed of two sections, which were numerically simulated based on the experimental condition described above. With a 3.5 GHz chirping bandwidth on each section and 1 μs pulse width, the range resolution is approximately 4.28 cm. When waveforms of the two sidebands are combined, although the overall chirping bandwidth is doubled, the range resolution may not be improved if their phases are not continuous. Ideally, when the phase discontinuity is removed, the range resolution is improved to 2.13 cm, shown as the dotted line in Fig. 4.

Figure 5 shows the spectra of measured waveforms using the experimental setup shown in Fig. 1, in which the dashed and the dotted lines represent down-converted spectra of the upper and the lower sidebands, and the spectral width of the central peak is approximately 1.52 MHz, corresponding to a range resolution of 4.4 cm. The solid line in Fig. 5 shows the spectrum of the combined waveform with matched phase, and the spectral width is reduced to 0.8 MHz, corresponding to a range resolution of 2.3 cm.

A more systematic measurement was then performed by moving the target along a sliding rail so

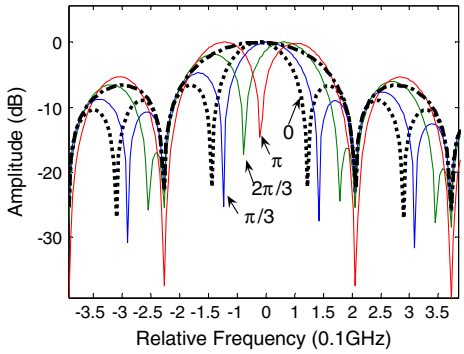

Fig. 4. Impact of phase discontinuity on range resolution using only one sideband (dashed line), using combined waveforms of two sidebands but with different phase discontinuities (solid lines), and continuous phase (dotted line).

that the time delay could be varied progressively. In order to eliminate the ambiguity due to the periodic nature of the optical pulses and the time delay due to the instrument, we used the reflection from the second output arm of the fiber coupler as a fixed-distance reference, as shown in Fig. 1, so that the range information of the target could be calibrated. The side peak in the spectrum of Fig. 5 at approximately 9 MHz is attributed to the reflection from the reference arm. Figure 6 shows the target range measured with the bandwidth efficient coherent lidar and the comparison with the actual distance of the target. Note that in many practical applications the target may not be stationary, and the moving speed of the target will introduce a Doppler shift on the return optical signal. This will have to be considered in the signal processing algorithm of phase continuity and target range calculation.

In the system configuration demonstrated here, frequency down-conversion was performed in the RF domain so that the receiver has to have sufficient electric bandwidth, which is 4 GHz in our

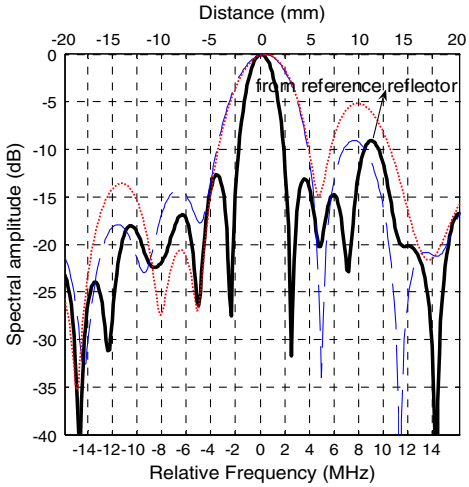

Fig. 5. Examples of measured spectra of a single sideband (dashed and dashed–dotted lines) and the combination of both sidebands after postprocessing (solid line).

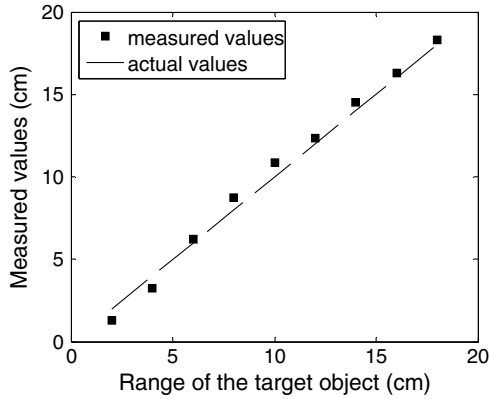

Fig. 6. Target range measured by bandwidth efficient coherent lidar versus the actual target distance.

experiment. Frequency down-conversion in the optical domain is also possible as previously demonstrated in Ref. [7] for an FMCW lidar system using coherent homodyne detection, where the receiver RF bandwidth can be much lower. Applying such a technique to the I/Q modulated lidar is an interesting direction to explore, which will require proper modification of the signal processing algorithm.

4. Conclusion

In this paper, we have demonstrated a bandwidth efficient coherent lidar which allows the doubling of modulation bandwidth efficiency through the simultaneous utilization of the I and Q components. The importance and the procedure to maintain RF phase continuity between linearly frequency-modulated I and Q components through digital signal processing have been discussed. Theoretical analysis and experimental verification indicate that this lidar configuration is able to half the range resolution compared to a conventional FMCW lidar with the same RF chirping bandwidth.

References

1. J. M. Vaughan, "Coherent laser spectroscopy and Doppler lidar sensing in the atmosphere," Phys. Scr. **T78**, 73–81 (1998).
2. C. J. Karlsson, F. Å. A. Olsson, D. Letalick, and M. Harris, "All-fiber multifunction continuous-wave coherent laser radar at 1.55 μm for range, speed, vibration, and wind measurements," Appl. Opt. **39**, 3716–3726 (2000).
3. M. Harris, R. I. Yong, F. Köpp, A. Dolfi, and J.-P. Cariou, "Wake vortex detection and monitoring," Aerosp. Sci. Technol. **6**, 325–331 (2002).
4. X. Mao, D. Inoue, S. Kato, and M. Kagami, "Amplitude-modulated laser radar for range and speed measurement in car applications," IEEE Trans. Intell. Transp. Syst. **13**, 408–413 (2012).
5. S. Gao and R. Hui, "Frequency-modulated continuous-wave lidar using I/Q modulator for simplified heterodyne detection," Opt. Lett. **37**, 2022–2024 (2012).
6. S. Gao, M. O'Sullivan, and R. Hui, "Complex-optical-field lidar system for range and vector velocity measurement," Opt. Express **20**, 25867–25875 (2012).
7. P. Adany, C. Allen, and R. Hui, "Chirped lidar using simplified homodyne detection," J. Lightwave Technol. **27**, 3351–3357 (2009).
8. R. V. Chimenti, M. P. Dierking, P. E. Powers, and J. W. Haus, "Sparse frequency LFM ladar signals," Opt. Express **17**, 8302–8309 (2009).
9. R. V. Chimenti, M. P. Dierking, P. E. Powers, J. W. Haus, and E. S. Bailey, "Experimental verification of sparse frequency linearly frequency modulated ladar signals modeling," Opt. Express **18**, 15400–15407 (2010).
10. P. A. Roos, R. R. Reibel, T. Berg, B. Kaylor, Z. W. Barber, and W. R. Babbitt, "Ultrabroadband optical chirp linearization for precision metrology applications," Opt. Lett. **34**, 3692–3694 (2009).
11. N. Satyan, A. Vasilyev, G. Rakuljic, V. Leyva, and A. Yariv, "Precise control of broadband frequency chirps using optoelectronic feedback," Opt. Express **17**, 15991–15998 (2009).
12. R. Huber, M. Wojtkowski, K. Taira, J. G. Fujimoto, and K. Hsu, "Amplified, frequency swept lasers for frequency domain reflectometry and OCT imaging: design and scaling principles," Opt. Express **13**, 3513–3528 (2005).